

Research paper

Investigation of at-vent dynamics and dilution using thermal infrared radiometers at Masaya volcano, Nicaragua

Yvonne K. Branan^{a,*}, Andrew Harris^b, I. Matthew Watson^{a,c}, J.C. Phillips^c,
Keith Horton^b, Glyn Williams-Jones^d, Harold Garbeil^b

^a *Geological & Mining Engineering and Sciences, Michigan Technological University, 1400, Townsend Drive, Houghton, MI, 49931, USA*

^b *HIGP/SOEST, University of Hawai'i, 1680 East-West Road, POST 504, Honolulu, HI, 96822, USA*

^c *Department of Earth Sciences, University of Bristol, Wills Memorial Building, Queen's Road, Bristol, BS8 1RJ, UK*

^d *Department of Earth Sciences, Simon Fraser University, 8888 University Drive, Burnaby, British Columbia, V5A 1S6, Canada*

Received 21 April 2005; accepted 31 July 2007

Available online 28 August 2007

Abstract

In order to develop a detailed understanding of the dynamics of gas puffing (gas release as a series of distinct pulses) and more sustained degassing (steady plumes of gas) during persistent volcanic degassing, measurements of gas mass flux are required in the vicinity of the volcanic vent. Masaya volcano (Nicaragua), a persistently degassing system, is an ideal location for measuring the dynamics of releases of volcanic gas in the first few seconds of their propagation. We carried out two field experiments during February 2002 and March 2003, during which thermal infrared thermometers were targeted into the degassing vent at Masaya to record thermal variations related to variations in the at-vent gas emission over short (on the order of seconds) time scales. The thermometers recorded an oscillating signal as gas puffs passed through the field of view, detailing variations in the degassing process developing over time scales of seconds. These data were processed to extract puff frequencies, amplitudes, durations, emission velocities and volumes. These data showed that, over time periods of hours, the total gas flux was stable with little variation in the puffing frequency. However, between the 2002 and 2003 data set we noted an increase in mean plume temperature, puffing frequency, puff emission velocity and puff volume, as well as a decrease in mean puff duration. These changes were consistent with a thermal data-derived increase in emitted gas flux from $4.2 \times 10^7 \text{ m}^3 \text{ d}^{-1}$ to $6.4 \times 10^7 \text{ m}^3 \text{ d}^{-1}$ between the two campaigns. Turbulent gas puffs entrain surrounding air, and quantifying the magnitude of air entrainment, or dilution, represents a major challenge for the measurement of total volcanic gas emissions. Our observations of small gas puffs suggest that they behave as turbulent buoyant thermals, and we use equations for mass, momentum and buoyancy, coupled with the standard entrainment assumption for turbulent buoyant flows, to estimate the gas puff dilution. The theoretically calculated dilution of 0.09 and 0.24 between emission and detection yields total SO_2 mass fluxes of 209 t d^{-1} and 864 t d^{-1} for 2002 and 2003, respectively. This compares well with UV-spectrometer SO_2 fluxes of 470 and 680 t d^{-1} for February 2002 and March 2003, respectively.

© 2007 Elsevier B.V. All rights reserved.

Keywords: persistent degassing; thermal; gas puff; gas/mass flux; Masaya

1. Introduction

A critical issue in the study of volcanic gas plumes is their near-vent behavior. Methods such as COSPEC

* Corresponding author. Tel.: +1 906 487 2531; fax: +1 906 487 3371.

E-mail address: ykbranan@mtu.edu (Y.K. Branan).

(COrrelation SPEctroscopy), DOAS (Differential Optical Absorption Spectroscopy) and FLYSPEC derive gas mass fluxes by using UV light to pass through the released gas (Stoiber et al., 1983; Galle et al., 2002; Horton et al., 2006). Typically, these measurements are made by observing the released gas from underneath and using sunlight as the UV source and are taken some distance downwind (e.g. Stoiber et al., 1983). The complex plume dynamics that operate between the vent and the measurement position mean that any short-term (on the order of seconds to minutes) signature associated with short-lived shallow sub-surface processes, such as convective overturn of a lava lake, gas-pistoning or gas bursting at the magma free surface, cannot be effectively quantified using these methodologies. Any of these mechanisms might introduce unsteady source conditions and generate puffs of gas in the volcanic plume.

The near-vent dynamics of volcanic gas releases, specifically emission velocity, expansion, entrainment and dilution of volcanic gases as they enter the atmosphere, are currently very poorly constrained. These factors are critical in determining the physico-chemical environment for faster reacting species and govern reaction rates for the more reactive species in the first few seconds of exposure to the atmosphere. Being able to quantify near-vent plume dynamics and measure gas flux very close to the vent has the advantage that any signal associated with shallow sub-surface processes might be retained. However, the problem with conventional methods is the lack of a UV source when the instruments are pointed into volcanic craters to measure emission rates near to the vent. In this paper, we describe a new method of determining entrainment rates for weak volcanic plumes based on thermal infrared measurements at Masaya volcano, Nicaragua, develop the necessary mathematical framework for derivation of the entrainment rate, and discuss the use of these measurements in estimating emitted gas fluxes.

Masaya volcano provides an outstanding location to examine at-vent plume dynamics and degassing rates at a persistently active volcano. At Masaya, the Santiago Pit Crater hosts a single active vent emitting a persistent gas plume which can easily be targeted from the car park perched on the south rim of the crater (Fig. 1). The Santiago Pit Crater formed in 1858–1859 and hosts a semi-persistent degassing vent that exhibits variable levels of activity (Rymer et al., 1998). Since 1895, there have been at-least five periods of enhanced degassing (Stoiber et al., 1986). The most recent period of enhanced degassing began during 1993 when a vent hosting a lava lake and Strombolian eruptions became established on the floor of Santiago (Rymer et al., 1998; Williams-Jones

et al., 2003). As part of this most recent cycle, the data of Williams-Jones et al. (2003) indicate a 4 year long oscillation in degassing rates beginning during 1997 when COSPEC-derived SO₂ fluxes began to increase from a low of 350±260 t d⁻¹ in February 1997 (Williams-Jones et al., 2003 and unpublished data). This cycle reached a peak of 2170±790 t d⁻¹ during April 1998 before declining again to a low of 320±23 t d⁻¹ by May 2001. These cycles in the gas flux are known to occur at Masaya with a periodicity of 4–10 years, and have been proposed to reflect cycles of replenishment, degassing and convective overturn of magma in a shallow reservoir (Rymer et al., 1998; Williams-Jones et al., 2003).

During 2002 and 2003 we carried out two thermal experiments at Masaya to determine the entrainment rate and the stability of gas and mass fluxes over shorter (seconds to minutes) time scales. In Sections 2 and 3 below, we summarize the field experiment location and design and the results from the field study, respectively. In Section 4 we review the dynamics of turbulent buoyant finite-volume gas releases, and present a method for estimating the dilution of these flows by the ambient fluid into which they propagate. In Section 5 we use this method to make comparisons of the gas flux estimated from thermal infrared (TIR) data with COSPEC measurements at Masaya, and discuss general aspects of this approach.

2. Field location, experiment design and data processing

A small explosion at Masaya on April 23, 2001, opened a new 10-m wide vent at the southern edge of the Santiago pit crater (GVN, 2001 and Fig. 1). Thereafter, the old vent became inactive and gas emission persisted from the new (Southern) vent. Laser range finder measurements showed that by February 2002 this vent had attained a dimension of 70 m (N–S) by 90 m (E–W) (Fig. 2).

The experiment was located on the southern rim of the Santiago pit crater, from where the thermometers were targeted directly into the degassing vent (Fig. 2) at an angle of 45°. This gave a ~340 m long line of sight which, given the 1° field of view (FOV) of the sensors used and applying simple geometry (diameter=tan(FOV)×line of sight), meant that the integrated temperature for a circular area ~6 m in diameter was recorded. Data sets were collected over two periods during February 2002 and March 2003. The first data set was collected between 2 and 24 February 2002. This data set consisted of 34 separate data sets, each between 23 and 167 min long and acquired on 15 different days within the study period (Table 1). The total duration of

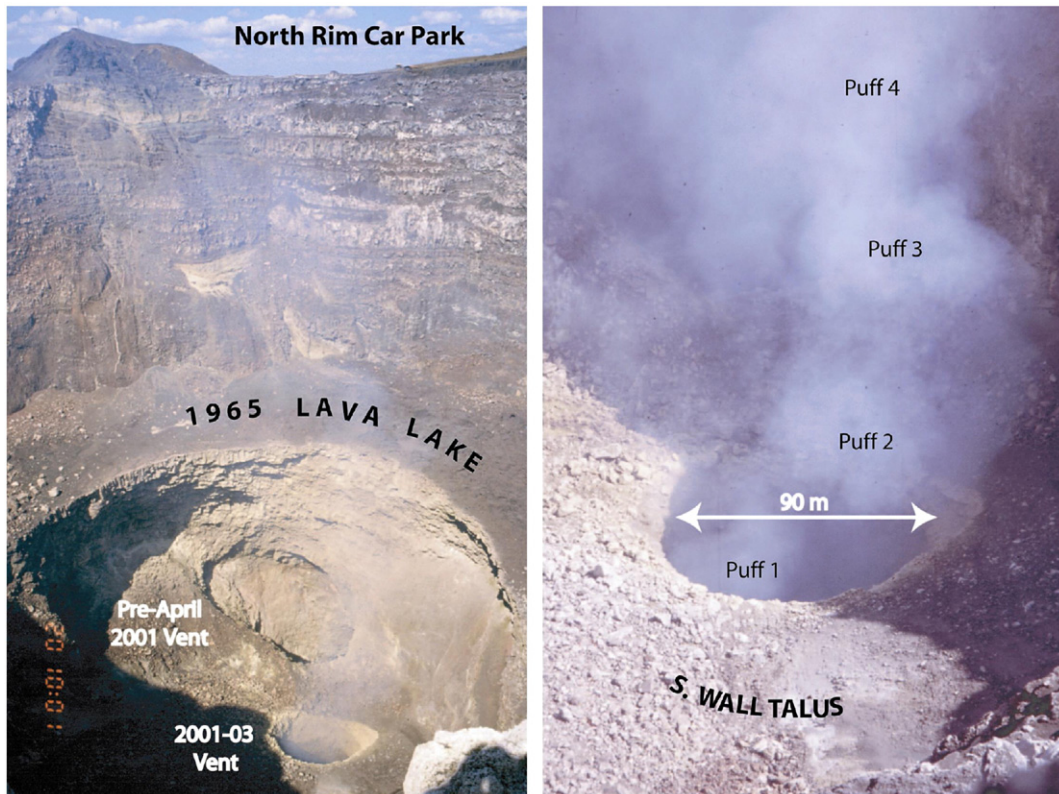


Fig. 1. Santiago Pit crater (Masaya) viewed from the measurement site on the southern rim. The active vent in 2002 and 2003 is enlarged on the right showing persistent, but puffing, gas emission.

this first data set was 74 h. The second was collected during 23–24 March 2003. This consisted of ten separate data sets, each between 68 and 167 min long and with a total duration of 26 h (Table 1). In all cases the instruments were pointed directly into the vent at an angle of 45° and targeted such that the central, highest temperature portion of the gas release rose directly through the sensor field of view.

The thermal infrared thermometers consist of a simple telescope, a broad-band ($8\text{--}14\ \mu\text{m}$) radiometer and portable data logger and have been deployed in several volcanic settings over the last few years to provide robust time series of thermal activity (e.g. Harris et al., 2005). Analog data are output as a continuous voltage which can easily be converted to brightness temperature (factory calibrated such that 1 mV equates to 1°C or 1°F). It should be noted that these temperatures must be considered as *brightness temperature* or treated in a relative (rather than absolute) manner, as the radiometers do not consider the emissivity of the target, or the contribution of mixed targets (such as a semi-transparent plume against wall rock).

During 2002 and 2003 gas emission from the active vent proceeded as a stream of gas puffs (Fig. 1). These

puffs leave a characteristic signal in time series of thermal data collected by thermal infrared (TIR) thermometers (see also Ripepe et al. (2002) and Harris and Ripepe (2007)). Specifically, passage of the gas puffs through the

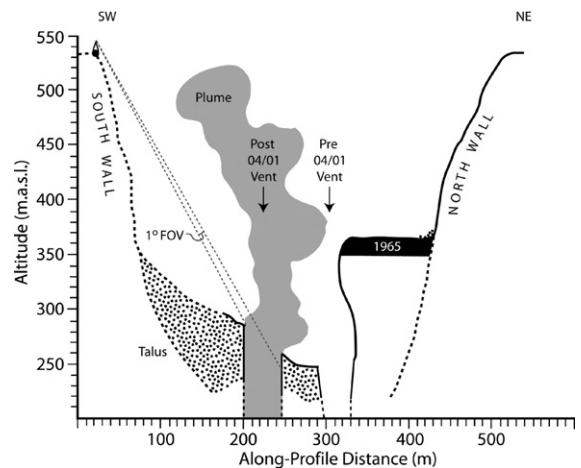


Fig. 2. NE–SW profile across Santiago Pit crater, obtained using a laser range finder located at the south rim measurement site during March 2003, showing the instrument line of sight and field of view.

Table 1
Individual data set characteristics. Sample rate is 1 s and all times are local

Date	Start time	Stop time	Duration (min)	Min. T (°C)	Max. T (°C)	Mean T (°C)	Standard deviation
2-Feb-02	9:09:18	11:43:33	154	–	–	–	–
2-Feb-02	11:43:58	13:00:45	77	–	–	–	–
4-Feb-02	11:44:05	14:30:33	167	–	–	–	–
8-Feb-02	7:37:32	10:09:18	152	–	–	–	–
8-Feb-02	10:09:49	12:41:35	152	–	–	–	–
8-Feb-02	12:49:51	15:36:29	167	–	–	–	–
10-Feb-02	10:44:10	13:29:26	165	–	–	–	–
11-Feb-02	10:11:11	12:57:49	167	44	94	62	14
11-Feb-02	12:59:16	15:45:54	167	46	99	65	14
11-Feb-02	15:46:31	16:40:57	54	48	104	65	16
12-Feb-02	9:45:49	12:32:27	167	46	93	61	12
12-Feb-02	12:32:55	15:19:33	167	48	97	68	14
13-Feb-02	9:51:37	10:47:52	56	55	113	83	22
16-Feb-02	9:56:18	12:39:17	161	36	157	89	64
16-Feb-02	12:52:46	15:39:24	167	89	149	117	16
16-Feb-02	15:46:38	17:07:44	81	94	143	116	14
18-Feb-02	8:57:52	11:44:30	167	88	136	112	13
18-Feb-02	11:45:00	14:31:38	167	86	140	112	13
18-Feb-02	14:32:00	17:18:38	167	93	142	113	13
19-Feb-02	14:14:01	15:57:41	104	85	204	100	14
20-Feb-02	9:40:47	12:27:25	167	86	140	113	9
20-Feb-02	12:39:42	15:26:20	167	80	138	109	11
20-Feb-02	15:27:19	16:16:53	50	86	151	115	10
20-Feb-02	16:22:34	17:09:31	47	83	146	112	12
21-Feb-02	9:58:05	10:20:50	23	82	145	106	12
21-Feb-02	10:22:34	13:09:12	167	72	168	126	9
21-Feb-02	13:09:34	14:32:28	83	108	174	134	8
22-Feb-02	9:03:36	11:35:32	152	100	171	129	8
22-Feb-02	11:35:48	14:22:26	167	109	183	136	9
23-Feb-02	9:21:35	12:08:13	167	91	162	126	9
23-Feb-02	12:09:19	13:20:19	71	105	164	131	8
23-Feb-02	13:26:46	16:13:24	167	31	171	91	45
23-Feb-02	16:15:43	17:06:53	51	88	152	120	11
24-Feb-02	14:37:42	16:53:55	136	91	149	118	9
23-Mar-03	10:32:36	11:06:32	68	111	177	143	11
23-Mar-03	11:11:29	12:34:48	167	111	181	153	10
23-Mar-03	12:37:54	14:01:13	167	114	192	154	11
23-Mar-03	14:08:28	15:31:47	167	121	194	155	9
23-Mar-03	15:33:41	16:47:52	148	135	191	157	8
24-Mar-03	10:07:58	11:31:17	167	121	188	156	9
24-Mar-03	11:31:19	12:54:38	167	116	199	160	11
24-Mar-03	12:59:03	14:22:22	166	126	202	163	10
24-Mar-03	14:22:54	15:46:13	167	128	206	165	9
24-Mar-03	16:17:32	17:40:51	167	126	197	162	11

instrument's FOV results in an oscillating temperature signal which increases as each puff rises into the FOV and then declines again as the puff exits the upper edge of the FOV (Fig. 3).

The puffs can also be recorded in gas time series where they are apparent as oscillations in the SO₂ column amount (Fig. 4). However, a limitation of ultraviolet SO₂ measurements (e.g. Fischer et al., 2002; Edmonds et al., 2003) is that taking measurements requires a line of sight

with the sky as the background. In the case of Masaya, where the degassing source is located on the floor of a ~350 m deep and ~490 m wide pit crater, direct measurements of the gas path length concentration as it leaves the vent are impossible. As a result, the thermal versus gas column amount comparison given in Fig. 4 had to be obtained by targeting the plume which forms from merging of the near-discrete gas puffs, with the sky as a background. This measurement was made approximately

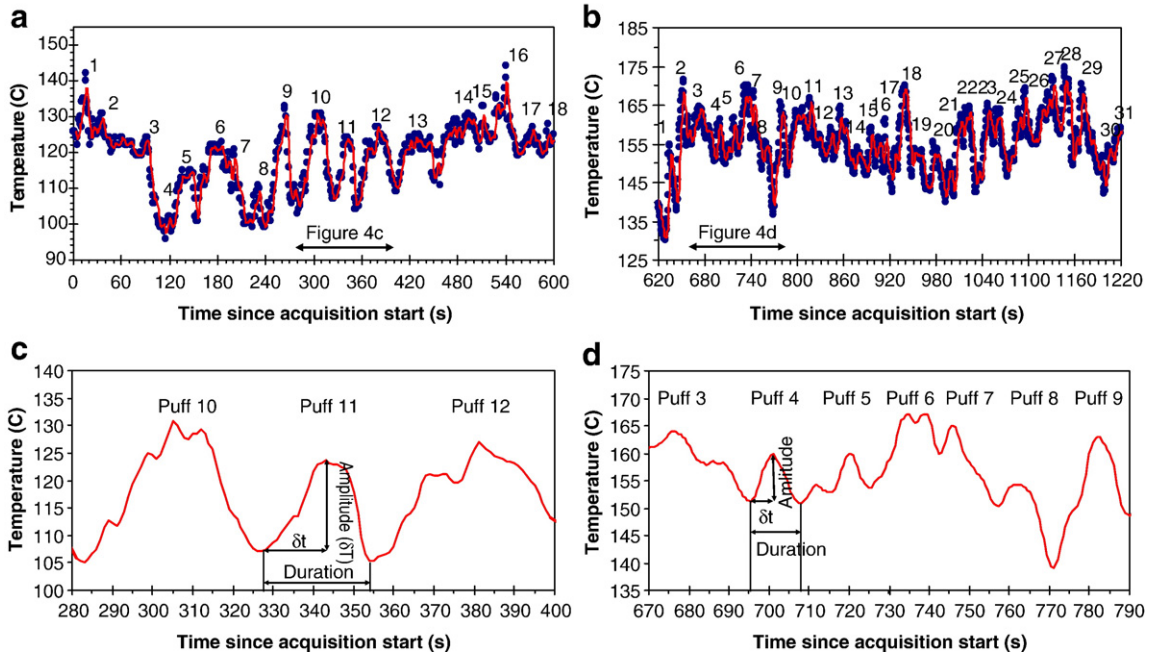


Fig. 3. Ten-minute-long data segments taken from (a) February 20, 2002 and (b) March 23, 2003 showing thermal oscillations recorded due to the passage of gas puffs through the thermal infrared thermometer field of view. Puffs are identified and numbered to show a higher frequency, as well as increased level of thermal signal, in 2003 over 2002. As indicated on (a) and (b), 2-min-long segments have been extracted from the 2002 (c) and 2003 (d) data sets. These are used to show the main puffing parameters extracted, as well as to illustrate the differences in duration and of the thermal pulses between 2002 and 2003, being typically of shorter duration and lower δT (i.e. faster) in 2003 than in 2002.

1 km downwind from the vent; this being the closest location to the vent at which the gas sensor (a FLYSPEC, Horton et al., 2006) could be adequately targeted.

At distances of 1 km downwind, much information regarding the short-period behavior and dynamics of the plume and degassing has been lost. At Masaya, puffs

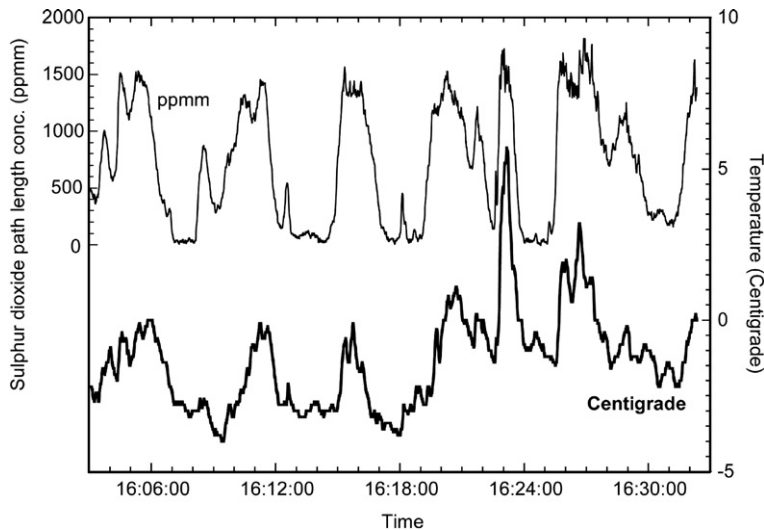


Fig. 4. SO_2 path length concentration (ppm m) and relative plume temperature ($^{\circ}\text{C}$) for the Masaya gas plume. For this experiment, the persistent gas plume was targeted ~ 1 km downwind of the source. The correlation between the raw SO_2 and thermal data (when smoothed to 40 s) is $T=0.002 \text{ ppm m}-2.827$ ($R=0.7$). The correlation between the first derivative between the SO_2 and thermal data (when smoothed to 40 s) is $\delta T=0.002 \delta \text{ppm m}+0.014$ ($R=0.8$).

Table 2

Summary of extracted puffing parameters for each data set. Frequency is in puffs per minute; amplitude is a one-minute average

Date	Data set	Frequency				Amplitude				Duration (s)			
		Min	Max	Mean	Std Dev	Min	Max	Mean	Std Dev	Min	Max	Mean	Std Dev
2-Feb-02	1	4	10	6.31	1.23	0	80	12.96	8.93	2	33	9.78	4.32
2-Feb-02	2	4	10	6.20	1.14	0	103	13.52	9.64	2	33	9.90	4.27
4-Feb-02	1	3	9	5.92	1.30	0	60	11.26	7.96	2	27	10.50	4.46
8-Feb-02	1	3	9	5.82	1.41	0	83	11.88	8.11	2	34	10.81	4.91
8-Feb-02	2	2	9	5.93	1.25	0	70	12.76	8.57	2	34	10.48	4.58
8-Feb-02	3	2	10	6.10	1.38	0	77	14.04	9.62	2	36	10.25	4.65
10-Feb-02	1	3	10	6.47	1.46	0	73	14.23	9.37	2	35	9.67	4.19
11-Feb-02	1	3	9	6.19	1.32	0	51	10.12	6.86	3	37	10.05	4.84
11-Feb-02	2	2	10	6.28	1.48	0	53	10.17	6.29	2	46	9.96	4.37
11-Feb-02	3	4	9	6.50	1.34	0	39	9.88	6.55	3	28	9.55	4.24
12-Feb-02	1	3	10	5.92	1.44	0	38	8.75	5.87	2	38	10.70	4.86
12-Feb-02	2	2	10	5.81	1.41	0	45	9.07	5.83	2	31	10.75	4.72
13-Feb-02	1	3	9	6.04	1.44	0	47	10.56	6.67	2	32	10.37	4.77
16-Feb-02	1	3	11	6.50	1.50	0	54	7.49	4.82	2	37	9.59	4.20
16-Feb-02	2	2	9	5.92	1.41	0	54	10.62	6.59	2	29	10.55	4.67
16-Feb-02	3	3	9	6.02	1.27	1	45	10.18	6.09	2	33	10.35	4.72
18-Feb-02	1	3	9	5.81	1.23	0	43	8.59	5.44	2	34	10.23	4.83
18-Feb-02	2	2	10	5.71	1.35	0	47	9.72	6.17	2	38	10.32	4.92
18-Feb-02	3	2	10	5.84	1.41	0	47	9.11	5.64	2	34	9.94	4.38
19-Feb-02	1	2	9	5.96	1.33	0	53	9.33	5.63	2	34	10.37	4.70
20-Feb-02	1	3	9	6.01	1.26	0	37	6.39	3.91	2	35	10.37	4.88
20-Feb-02	2	2	9	6.00	1.38	0	28	7.17	4.19	3	34	10.53	4.43
20-Feb-02	3	4	9	5.96	1.19	0	29	7.20	4.19	2	29	10.36	4.73
20-Feb-02	4	3	9	5.85	1.40	0	25	7.24	4.14	2	28	10.58	4.93
21-Feb-02	1	5	11	6.74	1.32	0	20	5.23	3.43	3	20	8.96	3.75
21-Feb-02	2	3	11	6.58	1.38	0	28	6.86	4.09	2	27	9.21	3.92
21-Feb-02	3	4	10	6.82	1.27	0	40	6.76	4.10	2	26	8.88	3.75
22-Feb-02	1	4	9	6.69	1.22	0	24	6.14	3.66	2	39	9.14	4.03
22-Feb-02	2	3	11	6.83	1.34	0	25	6.16	3.72	2	31	8.82	3.71
23-Feb-02	1	3	10	6.11	1.33	0	38	5.96	3.64	2	33	10.24	4.46
23-Feb-02	2	4	9	6.53	1.23	0	20	4.77	2.52	3	31	9.47	4.22
23-Feb-02	3	4	9	6.25	1.32	0	52	5.33	3.34	2	29	9.95	4.12
23-Feb-02	4	3	9	5.65	1.25	0	24	6.97	4.11	2	33	10.97	5.11
24-Feb-02	3	3	9	6.04	1.33	0	33	6.53	3.84	2	40	10.33	4.64
23-Feb-02	1	4	10	6.62	1.37	3	16	7.91	4.82	5	16	9.21	4.20
23-Feb-02	2	3	10	7.41	1.40	2	14	7.04	4.32	4	15	8.41	3.82
23-Feb-02	3	3	12	7.39	1.66	2	15	7.14	4.57	4	15	8.55	3.97
23-Feb-02	4	4	11	7.41	1.55	2	15	7.26	4.33	4	15	8.50	3.94
23-Feb-02	5	5	11	7.82	1.47	2	13	6.62	3.95	4	14	9.32	3.67
24-Feb-02	1	5	10	7.37	1.52	0	31	8.32	5.20	1	28	8.46	3.97
24-Feb-02	2	5	11	7.64	1.44	0	37	7.81	4.91	1	31	8.09	3.65
24-Feb-02	3	3	11	7.65	1.67	0	37	7.84	4.86	2	25	8.17	3.76
24-Feb-02	4	4	11	7.51	1.56	0	42	8.27	5.26	1	26	8.31	3.81
24-Feb-02	5	4	12	7.47	1.84	0	36	8.50	5.29	2	33	8.56	4.06

exit the vent at a moderately high temperature (Table 1), velocity and frequency ($\sim 7 \pm 1$ puffs per min during 2002–2003, Table 2). The puff decelerates, cools and expands rapidly upon emission, with gas from multiple puffs collecting within the main crater. This collects and mixes within the pit crater to be released as a larger, secondary puff from the pit crater itself. Secondary puffing rises from the pit crater at a much lower velocity and frequency (~ 12 per hour, Fig. 4) than the primary,

vent-exiting puffs. These are then recorded by the instruments targeted 1 km downwind. Thus, to gain maximum information about the short-term variation in the characteristics of the gas stream exiting the vent and degassing dynamics we prefer to target the gas as it leaves the vent.

In addition, ultraviolet SO_2 measurements naturally require sunlight or a source of ultraviolet radiation to allow the SO_2 absorption spectra to be produced

Table 3
Puff velocity, diameter and volume statistics

Date	Set	Velocity				Puff diameter				Puff volume			
		(m s ⁻¹)				(m)				(m ³)			
		Min	Max	Mean	Std Dev	Min	Max	Mean	Std Dev	Min	Max	Mean	Std Dev
2-Feb-02	1	0.8	3.0	1.8	0.7	10	24	15	5	485	7238	2064	2120
4-Feb-02	1	1.2	3.0	1.6	0.6	10	21	15	4	524	4849	1946	1575
10-Feb-02	1	0.7	6.0	2.5	2.1	13	42	18	9	1150	38792	5902	11614
12-Feb-02	1	0.4	2.0	1.3	0.6	10	18	14	3	501	3054	1575	812
16-Feb-02	2	0.3	3.0	1.5	0.8	9	18	13	3	382	3054	1264	814
18-Feb-02	2	0.9	3.0	1.3	0.6	10	19	13	3	524	3591	1356	900
20-Feb-02	3	0.5	6.0	2.6	1.6	3	40	14	6	21	33510	2723	5716
21-Feb-02	3	0.7	2.0	1.3	0.5	12	17	13	2	905	2352	1348	596
22-Feb-02	2	1.2	6.0	2.5	1.4	10	24	16	5	524	7238	2840	2480
24-Feb-02	1	0.5	3.0	1.5	0.7	10	22	14	4	496	5575	1729	1486
Totals		0.3	6.0	1.8	1.0	3	42	15	4	21	38792	2275	2811
23-Mar-03	1	0.4	6.0	3.2	1.6	7	32	15	5	192	17809	2211	2789
23-Mar-03	2	1.3	6.0	2.9	1.5	12	24	19	4	982	7238	4086	2187
23-Mar-03	3	1.4	6.0	2.5	1.4	11	21	15	3	712	4558	2027	1388
24-Feb-03	1	1.1	8.0	3.6	2.3	11	27	17	5	697	10306	3052	3147
24-Mar-03	2	1.0	4.8	3.0	1.3	10	26	16	6	485	9634	2889	3135
Totals		0.4	8.0	3.1	1.6	7	32	16	5	192	17809	2853	2529

(Stoiber et al., 1983). Thermal data, however, can be collected by day or night, allowing generation of more complete (longer-duration) time series. Hence we targeted a varying (1–3) number of thermal infrared thermometers directly into the vent within Santiago and used the derived thermal time series to record the frequency and amplitude of the gas puffing (Fig. 3). Following Ripepe et al. (2002) and Harris and Ripepe (2007), these parameters were used as a potential proxy for degassing rates, allowing us to track short-term (second-to-hour-long) variations in the gas stream as it exited the vent.

Data were then processed to extract puff frequencies, amplitudes and durations using software written in IDL at the Hawaii Institute of Planetology and Geophysics. These results are summarized in Table 2. The software (peakstat.pro) identifies puffs as follows. First the data are smoothed to 2 s intervals. A puff is then identified from any positive change (increase) in temperature that exceeds a threshold value (for this data set 1 sample) and which lasts for more than a specified period of time (for this data set 2 samples). The puff termination is then identified by the next positive change. The puff duration (peak-to-peak and trough-to-trough distances), amplitude and time are then saved, and the puffing frequency in puffs per minute is calculated. This automated puff statistic extraction procedure was checked against manual picking to reveal an accuracy of around ± 2 puffs/min.

On 8 days during the 2002 experiment we also ran between 2 and 4 thermal infrared thermometers side-by-

side. This allowed us to (1) check the effect of slight differences in targeting on our results, and (2) check the extracted puffing statistics across multiple data sets. We found good agreement across all simultaneously collected data sets.

Puff velocity, diameter and volume were calculated manually following the methodology of Harris and Ripepe (2007) (Table 3). Puff velocity is calculated by dividing the vertical distance the puff has to travel across the FOV by the time (δt) it takes for the puff leading edge to move across the FOV (Harris and Ripepe, 2007). This distance is given by dividing the field of view (6 m) by the cosine of the look angle (45°) and for these experiments is 8.5 m. Time, δt , was defined by the time taken for the thermal signal at the onset of the puff to increase to a maximum, i.e. the first derivative of the thermal pulse or the trough-to-peak time (Fig. 3c–d). The assumption is that the thermal signal will increase as the leading edge of the puff moves across the field of view, increasingly filling the FOV and hence increasing the recorded temperature. Temperature will reach a peak once the puff leading edge has reached the top of the FOV, at which point the FOV is optimally filled. Thus, the rate at which the temperature increases at the beginning of each puff event is a function of the velocity at which the puff moves through the FOV. By multiplying the velocity by the puff duration (Fig. 3), puff diameter (in meters) can now also be calculated. Finally, by assuming a spherical shape, puff volume (in m³) can be calculated from this diameter (Table 3).

3. Results: short-term variations in puffing frequency

Puffing frequencies and puff durations were extremely consistent across both the 2002 and 2003 data sets (Fig. 5a). Throughout the 2002 data sets, mean puffing frequency and puff duration were stable at 6 ± 1 puff per min and 10 ± 4 s, respectively (Table 2). Frequencies and durations were equally stable across the 2003 data sets. Mean frequency had, however, increased slightly to 7 ± 2 puffs per min and puff duration had decreased to 8.5 ± 4 s (Table 2) but it is worth noting that these are within error.

Brightness temperatures recorded for the gas plume as it exited the vent and puff amplitudes were more variable (Fig. 5b). Brightness temperature and puff amplitude, respectively, were 105 ± 15 °C and 9 ± 6 °C in the 2002 data. Brightness temperatures were significantly higher (157 ± 10 °C) and puff amplitudes were slightly lower (8 ± 5 °C) in the acquisition period in 2003 (Tables 1 and 2). Day-to-day variation in plume temperature and amplitude recorded by a thermal

infrared thermometer, as shown in Fig. 5b, may reflect variations in external factors such as clarity of the atmosphere, ambient temperatures, humidity, condensation, mixed pixel effects, etc. Day-to-day variations may thus be forced by differences in factors such as humidity, condensation, extent of solar heating of ambient surfaces and/or the relative mix of ambient surfaces, heated vent-wall rock and gas plume within the sensor field of view.

The stability in puffing frequency within a particular day is illustrated in Fig. 6 using data collected over a ~6-h-long period during February 11, 2002 and over ~7-h-long period during March 24, 2003. These two data sets show that, for any particular period during the 2002 or 2003 data acquisition period, puff frequency was remarkably stable. The same stability over each period is also evident in the thermal amplitude data (Fig. 7).

To summarize, the thermal signal recorded for the gas exiting the vent at Masaya during 2002–2003 was highly variable over a time scale of seconds (Fig. 3) due to the emission of gas as a stream of distinct puffs

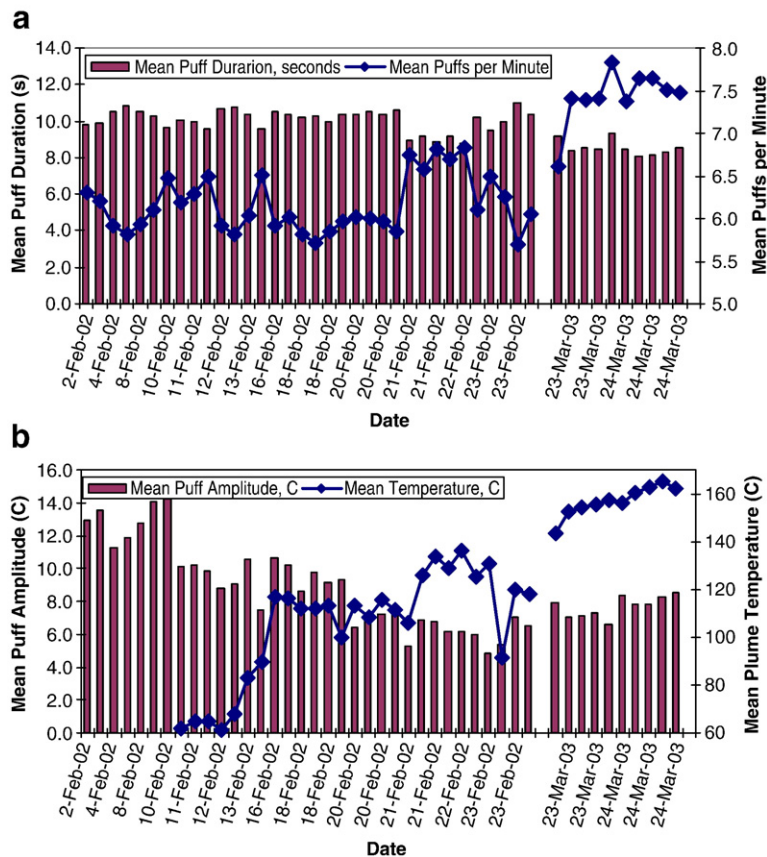


Fig. 5. (a) Mean puff duration and puff frequency for each data set listed in Table 1. (b) Mean puff amplitude and relative temperature for each data set listed in Table 1. Note that the x axis is not linear time and there are multiple entries on some days.

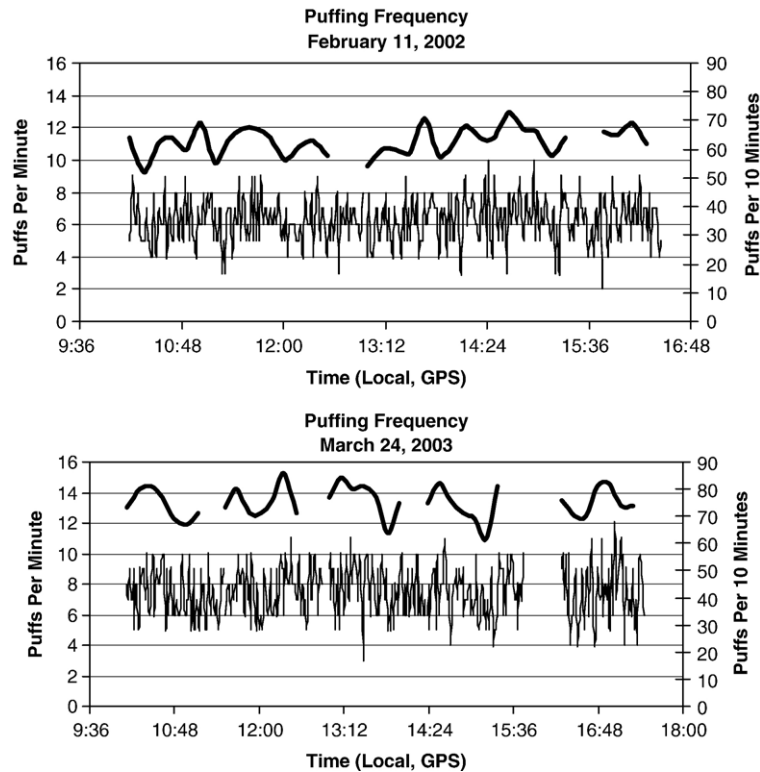


Fig. 6. Puff frequencies for the February 11, 2002 and March 24, 2003 data sets. Frequencies are given as puffs per 10 min (thick line) and puffs per minute (thin line).

(Fig. 1). Over time scales of several hours to a few days the frequency at which puffs are emitted is extremely stable, suggesting stable gas emission over such time scales. An increase in gas flux was observed between 2002 and 2003 (Williams-Jones et al., 2003). This is also suggested in the volume data we derive, although it is somewhat of a stretch to suggest a systematic change at these time scales with only a few days data per year. Instead, each data set will be treated separately in the following calculations. We now develop an appropriate methodology for estimating the gas flux from our thermally-derived gas puff volumes and rise velocities, by considering the dynamics of finite releases of buoyant gas into the atmosphere.

4. The rise dynamics and dilution of short duration buoyant gas releases

In the following analysis, we treat gas puffs as short duration, finite-volume buoyant releases of volcanic gas, consistent with our field observations of distinct volumes of higher temperature gas passing through the thermal radiometer field of view, approximately 5–10 m

above the volcanic vent. The puffs of higher temperature gas were interspersed with lower temperature regions interpreted to be atmospheric air between successive volcanic gas puffs (Fig. 3). Fig. 1 shows a direct visual observation of gas puffing at Masaya that provides support for this interpretation. First we investigate the flow regime of gas puffing at Masaya, in order to constrain the conditions for dilution of gas puffs by the surrounding air. In the analysis that follows, a robust one-dimensional description of buoyant turbulent motion (Morton et al., 1956; Turner, 1979) is used to investigate gas puff dilution. This approach has been successfully applied to a wide range of environmental and volcanological applications, and can provide a robust approximation to complex three-dimensional turbulent flows.

At the outset, we note that the major uncertainties in the calculations arise from uncertainties in the properties of the gas mixture and temperature.

William-Jones (2001) compiled gas flux data from Masaya in order to provide annual outputs of SO_2 , H_2O , CO_2 , HCl and HF , and from these values, the long-term average gas volume ratio can be determined as

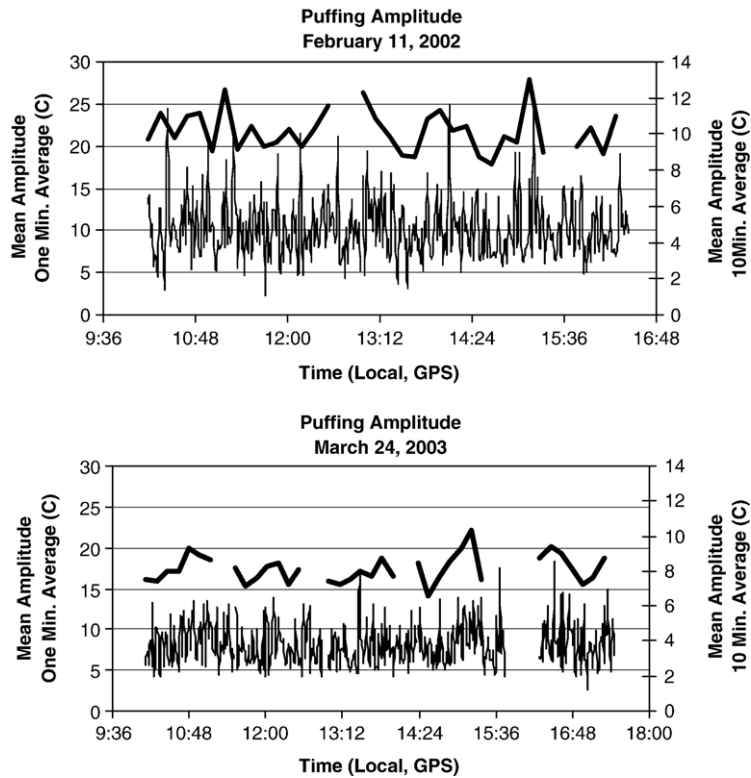


Fig. 7. Puffing amplitudes for the February 11, 2002 and March 24, 2003 data sets. Mean amplitudes are given across 10-min-long (thick line) and 1-min-long (thin line) periods.

4.5:86.8:6.9:1.6:0.2. Assuming this mixture behaves as an incompressible perfect gas, its density can be estimated using the perfect gas law for a multicomponent mixture (Kay and Nedderman, 1985). We estimate that the gas puff density at the source (prior to entrainment of surrounding air taking place), $\rho_p = 0.65 \text{ kg m}^{-3}$, taking $140 \text{ }^\circ\text{C}$ as typical of the average gas temperature (Fig. 3), textbook values of the densities and molecular weights of each component (Weast, 1967) and assuming the puff is at atmospheric pressure. The mixture density decreases only slightly to 0.60 kg m^{-3} if the average puff temperature is taken as $160 \text{ }^\circ\text{C}$ (Table 1). For comparison, the density of water vapor (the major component of the gas puff by volume) at $140 \text{ }^\circ\text{C}$ is 0.58 kg m^{-3} (Weast, 1967). To determine the puff flow regime, we estimate the value of the puff Reynolds number, $\left(\frac{u_p z \rho_p}{\mu_p}\right)$, taking the value of the puff velocity, u_p to be approximately 3 m s^{-1} (Table 3) and the height above the vent to be in excess of 1 m. There is no empirical formula from which to estimate the viscosity of the gas mixture that makes up the puff, so we estimate the puff viscosity as that of water vapor at $140 \text{ }^\circ\text{C}$ using standard properties of water

(Weast, 1967) and Sutherland’s formula (Saad, 1985) to find $\mu_p, \approx 2 \times 10^{-5} \text{ kg m}^{-1} \text{ s}^{-1}$. This approximation can be justified as the best available estimate, because the puff contains over 86% by volume water vapor. For heights greater than 1 m above the vent, we find that the Reynolds number of the puff is in excess of

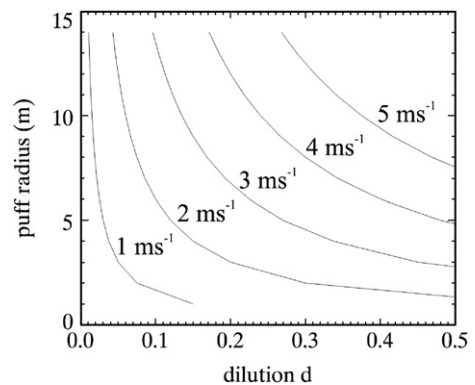


Fig. 8. Plot of entrainment rate versus puff diameter for a range of rise rates ($1\text{--}5 \text{ m s}^{-1}$).

10^4 , so the rising puff is fully turbulent, and will strongly incorporate, or *entrain*, atmospheric air. As a sensitivity test, we varied the viscosity over a range of reasonable values for different gas compositions for which textbook values could be found, and the calculated value of the Reynolds number only changed by a factor of two, remaining within the fully turbulent flow regime.

Rapidly released finite volumes of turbulent buoyant fluid are known as thermals (Turner, 1979; Sparks et al., 1998). Thermals are approximately spherical in shape (Scorer, 1957) and entrain ambient fluid through the action of a ring of vorticity along their edges (Turner, 1979), followed by rapid mixing of entrained fluid throughout the thermal. The properties of turbulent buoyant thermals vary self-similarly with distance from their source in a uniform environment, because the entrainment of ambient fluid is independent of the size and composition of the thermal (Turner, 1979; Sparks et al., 1998). In order to determine the emitted gas flux in gas puffs, we must determine the dilution of the gas puff, i.e. how much of the gas puff volume is entrained air at the height at which the thermal infrared measurements are made.

Following Morton et al. (1956), Turner (1979) and Sparks et al. (1998), the bulk motion of a discrete buoyant thermal can be described in terms of coupled equations for the conservation of mass, momentum and the buoyancy-generating property, denoted by C . If we assume that these properties are uniform across the rising thermal, and the changes in density in the thermal are much less than the density difference between the thermal and the atmospheric air, we can write these conservation equations as

$$\frac{db^3}{dz} = 3\epsilon b^2 \quad (1a)$$

$$3 \frac{d(b^3 w)}{dz} = \frac{2b^3}{w} g \frac{\rho_a - \rho_t}{\rho_{a0}} \quad (1b)$$

$$\frac{d(b^3(C_t - C_a))}{dz} = -b^3 \frac{dC_a}{dz} \quad (1c)$$

where b is the radius of the thermal, ϵ is the entrainment constant for the thermal, w is its vertical velocity, g is the acceleration due to gravity, ρ_a is the bulk density of the atmospheric air, ρ_t is the bulk density of the thermal, and C is the buoyancy-generating property such as gas concentration or enthalpy. The subscript 0 indicates the value of a property at the source of the gas thermal release, and the subscripts t and a denote values for the

thermal and the atmosphere, respectively. In an environment that is not stratified in density, such as the lowest layers of the atmosphere, Eqs. (1a)–(1c) have the solution

$$b = \epsilon z \quad (2a)$$

$$w = \left(\frac{B_0 b_0^3}{3\epsilon^3} \right)^{\frac{1}{2}} \frac{1}{z} \quad (2b)$$

$$B = g \frac{\rho_a - \rho_t}{\rho_{a0}} = \frac{B_0 b_0^3}{(\epsilon z)^3} \quad (2c)$$

where B is the buoyancy (Sparks et al., 1998). The entrainment constant ϵ cannot be determined theoretically, but has been measured experimentally to have a value $\epsilon=0.25$ for fully turbulent laboratory thermals (Scorer, 1957, Yamamoto, 2006).

The source conditions for gas puffing are typically not well constrained, as the source of the gas puff typically takes the form of a finite volume release from the magma surface which may be obscured or difficult to observe directly, and whose surface elevation may fluctuate (Ripepe & Gordeev, 1999; Ripepe et al., 2002; Harris and Ripepe, 2007). It is thus difficult to determine the parameters initial puff radius (b_0) and height above the source (z). In order to estimate the dilution of a gas puff (assuming that its behavior is analogous to that of a buoyant thermal as developed here) an appropriate methodology is to combine Eqs. (2a) and (2b) to eliminate the height, z . If we define the dilution of a gas puff as the ratio of the initial volume to the volume at the measurement height, and assume a spherical geometry, the dilution, d , can be written

$$d = \frac{(4/3)\pi b_0^3}{(4/3)\pi b^3} = \left(\frac{b_0}{b} \right)^3 \quad (3)$$

Substituting Eq. (2a) into Eq. (2b) and re-arranging, we find

$$b = \left(\frac{B_0 b_0^3}{3\epsilon} \right)^{\frac{1}{2}} \frac{1}{w} \quad (4)$$

so that

$$d = \left(\frac{b_0}{b} \right)^3 = \frac{3\epsilon w^2}{B_0 b} \quad (5)$$

The source buoyancy, B_0 , can be estimated from initial values of the gas puff density (0.65 kg m^{-3}) and the atmospheric density (1.25 kg m^{-3}) as having a typical value of about 5 m s^{-2} for our measurements. In 2002, the

measured gas puff radius had a mean of 10.5 m and a standard deviation of 3 m, and the measured gas puff velocity had a mean of 2.5 m s^{-1} and a standard deviation of 1.3 m s^{-1} (Table 3). These values correspond to a mean dilution $d=0.09$, with the limits of one standard deviation being $d=0.29$ and $d=0.02$. In 2003, these parameter values increased to a measured mean gas puff radius of 11.5 m and a standard deviation of 3.0 m, and the measured gas puff velocity had a mean of 4.3 m s^{-1} and a standard deviation of 2.3 m s^{-1} (Table 3). These values correspond to a mean dilution $d=0.24$, with the limits of one standard deviation being $d=0.77$ and $d=0.04$. From the form of Eq. (5), we see that the estimate of gas puff dilution is more sensitive to uncertainties in puff velocity than puff buoyancy or radius, and the large variation in the calculated dilution arises primarily from the variation in observed puff rise velocity (Table 3). Fig. 8 shows the variation of gas puff dilution with diameter and velocity over a range of typical values. The method outlined here enables the dilution of a discrete gas puff to be estimated independent of height above source, provided that the size and rise velocity can be measured, and the gas puff and environmental density can be estimated.

5. Discussion

If we take the mean gas puff radius obtained for 2002 (10.5 m s^{-1}) and 2003 (11.5 m s^{-1}) we can derive mean volumes of 4849 and 6370 m^3 for the two data sets respectively. If we then multiply the volumes by the typical puffing frequency for each day, (6 and 7 puffs/min for 2002 and 2003 data, respectively) we obtain gas volume fluxes of 4.2×10^7 and $6.4 \times 10^7 \text{ m}^3 \text{ d}^{-1}$. If we assume that the puff expands rapidly upon emission such that its density is approximately that of the surrounding atmosphere ($\sim 1.25 \text{ kg m}^{-3}$), this converts to 5.2×10^4 and $8.0 \times 10^4 \text{ t d}^{-1}$ of total gas per day in the 2002 and 2003 data set, respectively. This increase in emitted gas volume/mass tallies with the change in puffing style between 2002 and 2003 being forced by an increase in the gas flux, and is consistent with an increase in SO_2 flux from $\sim 470 \text{ t d}^{-1}$ in February 2002 to 680 t d^{-1} by March 2003 (Williams-Jones et al., unpublished data). This 2002–2003 increase appears to be part of an increasing trend in SO_2 flux at Masaya between 2002 and 2004.

As already discussed, gas flux data from Masaya have been compiled in order to provide annual outputs of SO_2 , H_2O , CO_2 , HCl and HF (William-Jones, 2001). Assuming from these gas ratios that 4.5 vol.% of each puff is comprised of SO_2 and using the gas volume fluxes given above SO_2 fluxes of 2350 and 3600 t d^{-1} for 2002 and 2003 can be derived.

These values are a little higher than measured values obtained on the same dates by Williams-Jones (unpublished data), but show the same order of increase as observed in these data. The overestimate results from the assumption that the total puff volume are comprised solely of volcanic gas, with no entrained air. Clearly, as a gas puff rises, expands and cools in the atmosphere, air entrainment will occur. Assuming the calculated entrainment rate (d) of 0.09 for 2002 and 0.24 for 2003 from the theory previously described and results detailed in Fig. 8, yields SO_2 fluxes of 209 t d^{-1} and 864 t d^{-1} , which are within error of the measured values of ~ 470 and 680 t d^{-1} (± 30 –60% error) obtained by Williams-Jones (unpublished data).

This study indicates some of the simplifications and difficulties in the estimation of atmospheric entrainment into volcanic gas puffs, which are themselves one of the less complex types of volcanic gas flow. Our observations suggest that they are distinct releases of buoyant volcanic gas that are characterized by uniform frequency of formation and rise speed over long time periods. As such, the dynamics of gas puffs are less complex than that of a low volume flux gas plume which may not have constant source flux conditions and may be emitted into an atmospheric wind of variable velocity.

Estimates of the gas puff Reynolds number suggest that under typical conditions for gas puffing, discrete gas puffs will be fully turbulent. This means that their dynamics and properties are self-similar (depending only on distance from their source) and this permits simplifications in the equations that describe their motion. However, turbulent flows are characterized by strong mixing with their environment, so the process of air entrainment into gas puffs cannot be neglected. The approach we use to estimate the dilution of gas puffs (Eq. (5)) requires measurement of the gas puff size and rise velocity, and specification of the gas composition. We note that a multi-instrumentation approach is thus required: thermal IR measurements as presented here provide gas puff size and velocity, and the temperature within the vent. An estimate of gas composition is required to constrain the gas puff density which is required to determine the source buoyancy flux; this can be recovered from FTIR measurements as here or possibly sampled directly at the vent. The gas puff density and viscosity are also required for the estimation of the Reynolds number that is used to assess whether the gas puff is fully turbulent. The use of a simplified estimate for viscosity is justified here as typically gas viscosities vary over a limited range (Weast, 1967), whereas the gas puff Reynolds number is an order of magnitude in excess of the critical condition for fully turbulent flow (Turner, 1979).

6. Conclusions

Thermal time series obtained from thermal infrared thermometers pointed into a degassing vent provide a means by which changes in the dynamics of the gas emission can be tracked over multiple time scales from seconds to years (Harris and Ripepe, 2007). Our good correlations between path length concentration and thermal amplitude during puffing at Masaya, as well as the coupled increase in puffing frequency and gas flux between our 2002 and 2003 data set, indicate that variations in the thermal characteristics of the plume and derived parameters (such as puff emission velocity and volume) can be used to track short- and long-term variations in degassing.

During both February 2002 and March 2003, we found no significant or abrupt changes in the frequency of puffing over periods of minutes-to-days. Such changes have, however, been observed in thermal and infrasonic data collected at Stromboli (Ripepe et al., 2002, 2004; Harris and Ripepe, 2007). This indicates a more steady degassing regime over periods of minutes-to-days at Masaya than at Stromboli, and may imply that the dynamical regime within the upper conduit at Masaya is somewhat more stable than Stromboli. At Masaya, during 2002–2003, for example, a steady flux of mass through the conduit may be responsible for the stable flow of gas from the vent evident in our data over these time scales. This is in contrast to the somewhat more cyclic behavior observed over similar time scales at Stromboli, where vents appear to move between phases of vigorous and weak degassing during minute-to-hour-long cycles (Ripepe et al., 2002; Harris and Ripepe, 2007).

Between 2002 and 2003, however, we observed an increase in the puff frequency and puff emission velocity, as well as an increase in temperature of the plume. This apparent increase in vigor of degassing, tallies with an increase in the calculated mass of gas emitted. The change in puffing rate thus appears to have been driven by an increase in magma, and hence gas flux, by a factor of ~ 1.5 . Both our thermal data and the gas flux data point to an increase in the SO_2 flux from c.a. 340 t d^{-1} in February 2002 to c.a. 770 t d^{-1} by March 2003.

In summary, thermal IR coupled with a theoretical approach provides estimates of gas flux near-vent which cannot be obtained by conventional gas flux measurements (e.g. COSPEC, DOAS FLYSPEC). Direct comparison with downwind COSPEC measurements at Masaya shows good agreement with the IR-radiometer derived SO_2 emission rate, although an estimate of volcanic gas composition is required for our method.

Thermal observations of gas puffing at Masaya show that, at this system during 2002–2003, degassing was highly variable over time scales of seconds, the gas being emitted from the vent as a series of distinct bursts. On an intermediate time scale of minutes-to-days our data reveals a much more stable system, indicating very little change in gas flux over such periods. On the longer term we note a steady change in gas flux. This tallies well with the long (four-to-ten-year) period oscillations in degassing already observed at Masaya by, for example, Rymer et al. (1998) and Williams-Jones et al., (2003). Indeed, the increase in gas flux measured by us between 2002 and 2003 appears to be part of an increasing trend that began around 2001 and was continuing as of 2004.

Acknowledgements

We are grateful to Dave Rothery and Lizzette Rodriguez for assistance with field data collection. YKB was funded via NSF Award 0118587 (P.I.: Bill Rose) and by a GAANN Fellowship through the Department of Education. HIGP contribution was funded by NASA grant NAG5-10640 under the EOS Program (P.I.: Peter Mouginiis-Mark) and by NSF grant EAR-0106349 (P.I.: Andy Harris).

References

- Edmonds, M., Herd, R.A., Galle, B., Oppenheimer, C.M., 2003. Automated, high time-resolution measurements of SO_2 flux at Soufriere Hills Volcano, Montserrat. *Bull. Volcanol.* 65, 578–586.
- Fischer, T.P., Roggensack, K., Kyle, P.R., 2002. Open and almost shut case for explosive eruptions: vent processes determined by SO_2 emission rates at Karymsky volcano, Kamchatka. *Geology* 30 (12), 1059–1062.
- Galle, B., Oppenheimer, C., Geyer, A., McGonigle, A., Edmonds, M., Horrocks, L., 2002. A miniaturised ultraviolet spectrometer for remote sensing of SO_2 fluxes: a new tool for volcano surveillance. *J. Volcanol. Geotherm. Res.* 119, 241–254.
- GVN, 2001. Masaya. *Bull. Glob. Volcanism Netw.* 26 (4), 11–14.
- Harris, A.J.L., Ripepe, M., 2007. Temperature and dynamics of degassing at Stromboli. *Journal of Geophysical Research* 112, B03205. doi:10.1029/2006JB004393.
- Harris, A., Pirie, D., Horton, K., Garbeil, H., Pilger, E., Ramm, H., Hoblitt, R., Thornber, C., Ripepe, M., Marchetti, E., Poggi, P., 2005. DUCKS: low cost thermal monitoring units for near-vent deployment. *J. Volcanol. Geotherm. Res.* 143, 335–360.
- Horton, K.A., Williams-Jones, G., Garbeil, H., Elias, T., Sutton, A.J., Mouginiis-Mark, P., Porter, J.N., Clegg, S., 2006. Real-time measurement of volcanic SO_2 emissions: validation of a new UV correlation spectrometer (FLYSPEC). *Bull. Volcanol.* 68, 323–327.
- Kay, J.M., Nedderman, R.M., 1985. Fluid mechanics and transport processes. Cambridge University Press, Cambridge, UK, pp. 228–229.
- Morton, B.R., Taylor, G.I., Turner, J.S., 1956. Turbulent gravitational convection from maintained and instantaneous sources. *Proc. R. Soc. Lond., A* 234, 1–23.

- Ripepe, M., Gordeev, E., 1999. Gas bubble dynamics model for shallow volcanic tremor at Stromboli. *J. Geo. Res.* 104, 10,639–10,654.
- Ripepe, M., Harris, A.J.L., Carniel, R., 2002. Thermal, seismic and infrasonic evidences of variable degassing rates at Stromboli Volcano. *J. Volcanol. Geotherm. Res.* 118, 285–297.
- Ripepe, M., Marchetti, E., Poggi, P., Harris, A.J.L., Fiaschi, A., Ulliveri, G., 2004. Seismic, acoustic, and thermal network monitors the 2003 eruption of Stromboli Volcano. *EOS* 85 (35), 329–332.
- Rymer, H., van Wyk de Vries, B., Stix, J., Williams-Jones, G., 1998. Pit crater structure and processes governing persistent activity at Masaya Volcano, Nicaragua. *Bull. Volcanol.* 59, 345–355.
- Saad, M.A., 1985. *Compressible Fluid Flow*. Prentice-Hall, Inc., New Jersey.
- Scorer, R.S., 1957. Experiments on convection of isolated masses of buoyant fluid. *J. Fluid Mech.* 2, 583–594.
- Sparks, R.S.J., Bursik, M.I., Carey, S.N., Gilbert, J.S., Glaze, L., Sigurdsson, H., Woods, A.W., 1998. *Volcanic Plumes*. John Wiley, New York. 574 pp.
- Stoiber, R.E., Malinconico, L.L., Williams, S.N., 1983. Use of the correlation spectrometer at volcanoes. In: Tazieff, H., Sabroux, J.-C. (Eds.), *Forecasting Volcanic Events*. Elsevier, Amsterdam, pp. 425–444.
- Stoiber, R.E., Williams, S.N., Huebert, B.J., 1986. Sulfur and halogen gases at Masaya Caldera complex, Nicaragua; total flux and variations with time. *J. Geo. Res.* 91, 12,215–12,231.
- Turner, J.S., 1979. *Buoyancy Effects in Fluids*. Cambridge University Press, Cambridge, p. 368.
- Weast, R.C. (Ed.), 1967. *Handbook of Chemistry and Physics*, 48th ed. The Chemical Rubber Company Press, Cleveland, Ohio.
- William-Jones, G., 2001. *Integrated geophysical studies at Masaya Volcano, Nicaragua*, Ph.D. thesis, The Open University.
- Williams-Jones, G., Rymer, H., Rothery, D.A., 2003. Gravity changes and passive SO₂ degassing at the Masaya caldera complex, Nicaragua. *J. Volcanol. Geotherm. Res.* 123, 137–160.
- Yamamoto, H., 2006. *Dynamics of entrainment into releases of buoyant fluid with application to volcanic degassing*. M.Sc. thesis, University of Bristol.